JAAS

U−Pb ID-TIMS geochronology using ATONA amplifiers

Journal:	*Journal of Analytical Atomic Spectrometry*
Manuscript ID	JA-ART-03-2020-000135.R1
Article Type:	Paper
Date Submitted by the Author:	18-May-2020
Complete List of Authors:	Szymanowski, Dawid; Princeton University, Geosciences Schoene, Blair; Princeton University, Geosciences

SCHOLARONE™
Manuscripts

U–Pb ID-TIMS geochronology using ATONA amplifiers

Dawid Szymanowski and Blair Schoene

Department of Geosciences, Princeton University, Guyot Hall, Princeton, NJ 08544, USA.
*E-mail: dszymanowski@princeton.edu; bschoene@princeton.edu

Abstract

We document the performance of new ATONA ('aA to nA') amplifiers installed on an Isotopx Phoenix thermal ionisation mass spectrometer (TIMS) at Princeton University and evaluate their suitability for high-precision analyses of Pb and U isotopes in pg- to ng-size samples characteristic for U–Pb geochronology. The new amplifiers are characterised by low and stable noise levels comparable to 10^{12}–10^{13} ohm resistors, response time < 0.5 s, exceptional gain stability < 1 ppm and a vast dynamic range theoretically allowing to quantify signals from aA (10^{-18} A) to nA (10^{-9} A) level. We measured a set of Pb standards, synthetic U–Pb solutions and natural zircons at currents of 2×10^{-16}– 2×10^{-12} A (corresponding to intensities of 20 μV –200 mV relative to a 10^{11} ohm amplifier) to assess the utility of ATONA in replacing ion counting for the smallest samples. The results show a clear precision benefit of using ATONA-Faraday detection over Daly ion counting for ion currents of > 10^{-14} A (1 mV relative to a 10^{11} ohm amplifier or ca. 60 kcps). As such currents are routinely achievable for major Pb peaks of interest ($^{205-208}$Pb) in natural samples containing more than ca. 10 pg Pb* (radiogenic Pb), we expect ATONA-Faraday detection to find broad applications in U–Pb geochronology. Its practical use for low-blank, radiogenic samples continues to require ion counting for ^{204}Pb, either with a fixed Faraday–ion counter gain or using a dynamic two-step (e.g. FaraDaly) method. Routine adoption of ATONA Faraday collection in place of ion counting for most major Pb and U isotopes has the potential to increase sample throughput and precision, both improving the accessibility of isotope dilution (ID)-TIMS geochronology and pushing this technique towards better reproducibility.

1   Introduction

U–Pb geochronology, relying on radioactive decay of U to Pb in U-bearing minerals such as zircon, underpins much of what is known about the absolute timing of events in the geological past. Of many historical and modern analytical tools employed to analyse U and Pb isotopes, isotope dilution thermal ionisation mass spectrometry (ID-TIMS) has been established as the golden standard of precision and accuracy for a wide range of key Earth science questions.[1-3] This method, dating back to first magnetic sector mass spectrometers[4,5] and early isotopic estimates of the age of rocks and the Earth[6-8], has seen continued use for high-precision geochronology applications, particularly facilitated by the advent of Teflon labware, miniaturisation of chemical separation methods and the resulting reduction in laboratory blanks[9,10]. As a result, the combination of modern ultraclean preparation with multicollector TIMS is capable of producing U–Pb dates with precision on

42   the order of < 0.1% for single zircon crystals and as little as 0.01% for a 2-sigma weighted

43   mean of several single-crystal dates.[2,11]

44   However, even this precise analytical technique is in constant need of developments that

45   can improve inter-lab reproducibility. The U–Pb community uses a common tracer solution

46   developed through the EARTHTIME initiative[12,13] which eliminates spike-related biases;

47   however, the level of inter-lab reproducibility of homogeneous standards does not always

48   match the internal repeatability of individual laboratories or the precision of single

49   analyses.[14] One stream of improvements is aimed at better understanding and unifying the

50   often empirically developed lab procedures, e.g., 'chemical abrasion' pre-treatment of

51   zircon crystals.[15-17] In parallel, incremental improvements in mass spectrometry technology

52   can make isotopic analyses more time-efficient and reproducible.

53   One recent advance in TIMS has been the advent of high-ohmic (particularly 10^{13} Ω)

54   resistors for Faraday cup amplifiers, pioneered by Thermo Fisher for the Triton TIMS and

55   employed since for a variety of isotopic systems: Sr, Nd[18], common Pb[19], Os[20], and U–

56   Pb[11,21]. Faraday cups with high-value resistors have comparatively low noise and are

57   therefore capable of detecting small ion beams that until recently were only accessible with

58   ion counting systems. Specifically for U–Pb analyses of single crystals of accessory

59   minerals, 10^{13} Ω amplifiers have been shown to expand the range of application of Faraday

60   cups to pg-size Pb samples[11,21], largely obviating the need to use single-collector ion

61   counting for many samples. Currently, most routine analyses of Pb isotopes for U–Pb

62   geochronology employ a single ion counter (SEM-secondary electron multiplier or

63   Daly/photomultiplier) peak-hopping between 5–8 masses and typically require 2–5 h

64   analysis time per sample. Moving away from ion counting for Pb isotopes has the potential

65   to significantly reduce analysis time, at the same time eliminating the need for, and biases

66   from, additional detector calibrations and associated corrections (e.g. dead time, detector

67   voltage, beam interpolation).

68   The most recent breakthrough in Faraday cup amplification is the new ATONA ('aA to nA')

69   amplifying technology developed by Isotopx Ltd. for use in both Phoenix TIMS instruments

70   and NGX noble gas mass spectrometers.[22] ATONA is a capacitive transimpedance amplifier

71   using a proprietary technology partially described in UK patents GB2552232 and

72   GB2552233. It relies on capacitors rather than high-gain resistors, which results in fast

73   amplifier response time, low noise and a large dynamic range, theoretically allowing to

74   quantify a range of beam sizes from a few aA (10^{-18} A) to nA (10^{-9} A). Similar to high-ohmic

75   resistors, ATONA has the potential of replacing ion counting as the method of choice for

76   the smallest beams (e.g. pg-level Pb in single zircons); however, it also allows analyses at

77   high intensities without the need to swap between amplifiers of different resistance value.

78   As the same performance is available on all Faraday channels, the new amplifiers should be

79 ideally suited to static collection in TIMS for isotopic systems that require a large dynamic

80 range e.g. U or Ca.

81 Here we explore the capabilities of a new ATONA system installed at Princeton University

82 in early 2019 as applied to high-precision U-Pb ID-TIMS geochronology. We performed a

83 variety of tests to describe the baseline and noise behaviour of our ATONA, its gain stability

84 and response time, and tested its performance in analyses of small Pb ion beams (10^{-16}–10^{-12} A) of Pb isotopic standards, synthetic U–Pb solutions and standard zircons. We present

85

86 optimised analytical protocols that maximise the use of ATONA-Faraday collection for both

87 Pb isotopes and U isotopes in pg- to ng-size samples relevant to single-crystal

88 geochronology.

89

2   Experimental

2.1   Materials

92 In order to test the performance of the new amplifiers and explore the low intensity limits

93 of their applicability to Pb isotopic measurements, we analysed multiple aliquots of the

94 NIST SRM 982 Pb isotopic standard. Precision and reproducibility of combined U–Pb

95 analyses of spiked samples were tested with a combination of natural zircons and synthetic

96 zircon-like solutions across a range of ages: zircon GZ7, EARTHTIME (ET) 2 Ga solution, and

97 EarlyTime (ET) 4567-R solution. GZ7 is a homogeneous Sri Lankan megacrystic zircon

98 previously analysed by five TIMS laboratories to a grand mean of 530.26 ± 0.05 Ma.[14] ET 2

99 Ga is a synthetic U–Pb solution prepared and distributed by Condon et al.[23] for inter-

100 laboratory comparisons within the framework of the EARTHTIME initiative. ET 4567-R is

101 the most radiogenic of a series of U–Pb solutions designed as interlaboratory standards for

102 labs dating early solar system materials using isochron methods.[24] All U–Pb samples were

103 mixed with the EARTHTIME ^{202}Pb–^{205}Pb–^{233}U–^{235}U (ET2535) mixed tracer[12,13] allowing for a

104 real-time mass fractionation correction.

105

2.2   Preparation and chemical separation

107 The natural zircon samples were pre-treated in order to minimise the effect of partial Pb

108 loss by following the chemical abrasion technique modified from ref. 15. Fragments of the

109 crushed megacryst GZ7 were annealed at 900 ºC for 48 h, rinsed with water and dilute

110 HNO_3 and leached in ~120 µl 29 M HF ('chemically abraded') for 12h at 180 ºC in individual

111 PFA microcapsules assembled in a Parr pressure vessel.[9] The leached zircon fragments

112 were transferred into individual 3 ml Savillex PFA beakers, fluxed in 6 M HCl for several

113 hours on a hotplate, then repeatedly rinsed in 4 M HNO_3 and loaded into their pre-cleaned

114 microcapsules with a microdrop of HNO_3 and ~90 µl 29 M HF. The samples were then

115   spiked with 5–20 mg of ET2535 tracer and digested in the Parr pressure vessel for ~60 h at

116   210 °C. The solutions were then dried down, redissolved in 6 M HCl at 180 °C in the oven to

117   convert to chloride form, and evaporated to dryness in preparation for ion exchange

118   chemistry. In order to reach smaller sample sizes while retaining routine sample/spike

119   ratios, six additional GZ7 samples were prepared by dissolving a single unspiked zircon

120   fragment which was then brought up in 6 M HCl, fluxed on a hotplate, split into aliquots of

121   various sizes, loaded into microcapsules, spiked, equilibrated in the oven at 180 °C, and

122   dried down for chemistry. Pb and U were separated through a miniaturised, HCl-based

123   anion exchange chemistry procedure on 50 µl columns modified from ref. 9; the resulting

124   U–Pb separates were dried down with a microdrop of 0.02 M H_3PO_4. The synthetic U–Pb

125   solutions (ET 2 Ga and ET 4567-R) were spiked, fluxed on a hotplate for several days to

126   ensure equilibration, then aliquoted into individual beakers and dried down with H_3PO_4. For

127   mass spectrometry, all U–Pb fractions were loaded on single zone-refined, outgassed Re

128   filaments with a drop of a silica gel emitter prepared following Gerstenberger and Haase[25].

129   The total blank including all reagents and sample handling from dissolution to filament

130   loading was determined periodically over the course of this study (n = 10), with an average

131   of 0.13 ± 0.03 pg Pb, 0.02 ± 0.01 pg U and a long-term average composition of $^{206}Pb/^{204}Pb$ =

132   18.63 ± 0.32, $^{207}Pb/^{204}Pb$ = 15.80 ± 0.23, $^{208}Pb/^{204}Pb$ = 38.54 ± 0.38 (1 standard deviation).

133

2.3   Mass spectrometry

135   All analyses were performed with an Isotopx Phoenix thermal ionisation mass spectrometer

136   installed in March 2019 at Princeton University. The mass spectrometer is equipped with an

137   axial Daly–photomultiplier ion counting system and 9 Faraday collectors connected to the

138   new ATONA amplification system. Faraday cup efficiency was established after installation

139   using analyses of SRM 982 Pb performed in dynamic mode and adjusting Faraday

140   efficiencies to minimise ratio residuals relative to the isotopic composition of ref. 13.

141   Efficiencies were kept constant over the course of this study. To generate a large test

142   dataset, inter-channel gain was updated ~3 times every week in a standard 4 h calibration

143   routine provided in the mass spectrometer control software.

144

Pb isotopes

146   Pb isotopes were acquired in two Faraday cup configurations intended for static analysis of

147   common Pb (SRM 982) and for mixed Faraday–Daly ('FaraDaly') analyses of (^{202}Pb–)^{205}Pb-

148   spiked zircon samples (Table 1). The 'zircon' configuration was designed to accommodate

149   all relevant Pb and UO_2 masses without the need to move any cups. As a consequence, we

150   did not analyse masses 201 and 203 which are often acquired in ion counting sequences to

151   monitor potential inferences from Tl and $BaPO_4$ (ref. 26); however, independent tests using

152   Daly ion counting on natural zircons showed negligible interferences from these species in

153   the current analytical setup. The zircon configuration did not use the axial Faraday cup,

154   which was moved away from the axial position in order to acquire the low-intensity ^{204}Pb

155   with the Daly-photomultiplier (PM). This requires either an assumption of a fixed Faraday–

156   Daly gain to obtain accurate $^{20x}Pb/^{204}Pb$ ratios, or its real-time correction; we used a shorter

157   second acquisition step (S2) with ^{205}Pb measured in the axial Daly to derive an accurate

158   gain by comparing $^{206}Pb/^{205}Pb$ between S1 and S2. The Faraday–Daly gain obtained from

159   this correction may vary by a few per cent during the course of an analysis so the

160   assumption of fixed gain would not be justified. SRM 982 analyses had variable baseline

161   length (30–1000 s), timing (e.g. every block vs single at start) and on-peak integration times

162   (10–100 s). All Pb signals for zircons and synthetic solutions were acquired with our

163   optimised integration time of 30 s on S1, 10 s on S2 and three baselines at start measured

164   for 300 s on axial masses 203.5, 204.5, and 205.5 (choice of baselines and integration times

165   discussed later). The Daly system was monitored with periodic measurements of SRM 982

166   used to correct for dead time and thus ensure its linearity over a range of intensities up to

167   2.5 Mcps.

168

U isotopes

170   The cup configuration (Table 1) was designed for static Faraday analyses of ^{233}U–^{235}U-

171   spiked samples as oxides, acquiring four isotopologues of UO_2 in cups L5–L2: $^{233}U^{16}O_2$,

172   $^{235}U^{16}O_2$, $^{238}U^{16}O_2$, and $^{269}(UO_2)$ used to correct for interferences of ^{18}O-bearing oxide

173   species. All UO_2 analyses were run at 30 s integration time, with a pair of 300 s baseline

174   measurements at the start on either side of the peak (axial mass 272.7 ± 0.5).

175   Acquiring $^{269}(UO_2)$ allowed us to correct for interferences of $^{233}U^{18}O^{16}O$ and $^{233}U^{16}O^{18}O$ on

176   mass 267 ($^{235}U^{16}O_2$ peak) inherent to ^{233}U–^{235}U spikes. While this and similar oxide

177   interferences can be corrected by assuming a blanket atmospheric value of $^{18}O/^{16}O$ (e.g.

178   Nier[27]), it has been shown that the oxygen isotopic composition of oxide species inside a

179   TIMS source might significantly diverge from atmospheric and evolve over the course of an

180   analysis.[28, 29] Therefore, accurate high-precision UO_2 analyses should ideally employ a

181   within-run correction with an $^{18}O/^{16}O$ value determined by comparing a pair of ^{18}O- and ^{16}O-

182   bearing UO_2 species acquired in real time.[11,12] The correction used here takes advantage of

183   the ability of the ATONA to quantify the small ^{18}O species beams in any Faraday cup, which

184   avoids acquiring it in the (typically axial) ion counter or to account for ion counter–Faraday

185   gain. Previous approaches used $^{272}(UO_2) = {}^{238}U^{18}O^{16}O + {}^{238}U^{16}O^{18}O$ measured either with a

186   Faraday cup or an axial ion counter.[11,12] We chose to acquire $^{269}(UO_2) =$

187   $^{235}U^{18}O^{16}O + {}^{235}U^{16}O^{18}O + {}^{233}U^{18}O^{18}O$ which, compared to $^{272}(UO_2)$, has the advantage of

188 being independent of sample size. The peak of $^{269}(UO_2)$ is generated primarily by ^{235}U-

189 bearing species so its intensity is mostly controlled by the amount of ^{235}U spike added.

190 Granted sufficient ionisation, this method should work for every routine ^{233}U–^{235}U-spiked

191 U–Pb sample with a typical 1–3 ng ^{235}U. All algorithms for this correction are provided in the

192 Appendix.

193

2.4   Data reduction

195 All data reduction for U–Pb analyses was performed using Tripoli and Redux software[30],

196 which uses the algorithms of McLean et al[31]. Pb analyses were corrected for instrumental

197 mass fractionation in real time using the ^{202}Pb/^{205}Pb of the ET2535 double spike[12] and a

198 linear mass fractionation law. SRM 982 Pb isotopic ratios were normalised to ^{208}Pb/^{206}Pb =

199 1.000249 (ref. 13). U isotope ratios were corrected for mass fractionation offline after the

200 UO_2 interference correction, using the measured ^{233}U/^{235}U relative to the double spike

201 composition[12] and sample ^{238}U/^{235}U of Hiess et al[32]. All U–Pb ratios and dates were

202 calculated relative to the spike ^{235}U/^{205}Pb [12] using the decay constants of Jaffey et al[33]. All

203 uncertainties are reported at the 2s level and do not include systematic uncertainty

204 components of ET spike composition or the decay constants.

205

3   Results and discussion

3.1   Baseline and noise

208 The ability to accurately measure small (<10^{-14} A) ion beams with Faraday cups is

209 fundamentally limited by the baseline and noise performance of a detector system. The

210 ATONA, which is kept at low vacuum and Peltier-cooled to -20 ºC, is characterised by low

211 noise comparable in magnitude to traditional design, high-ohmic, resistor-based amplifiers

212 (Fig. 1). The trajectory of improvement in ATONA amplifier noise with increased

213 integration time is oblique to theoretical bounds of Johnson–Nyquist noise for a given

214 fixed-resistivity amplifier; the noise decreases linearly with time rather than with the square

215 root of time. The combination of ATONA with the Phoenix cup design produces noise that

216 exceeds the theoretical limit for 10^{12} Ω resistors at integration times > 10 s and approaches

217 the theoretical limit for 10^{13} Ω resistors for integrations > 100 s (Fig. 1). The longest

218 integrations should therefore allow to quantify (with a signal/noise ratio of 10) beams as

219 small as 10 aA (10^{-17} A) or ca. 60 cps. Shorter integration times < 60 s that are more practical

220 for unstable signals can potentially access a range of beams of > 10^{-16} A (> 600 cps).

221 The baseline and noise behaviour of our ATONA is stable over periods comparable to the

222 length of a single measurement i.e. 1–2 h (Fig. 1) but it also shows remarkable

223 reproducibility over long periods. We have monitored both parameters by repeatedly

224   acquiring 1 h of electronic baseline over the course of the first 10 months of instrument use

225   (Fig. 2). After initial settling, both parameters reached a stable level which has remained

226   invariable. The only exception was a period of drift in noise in November (Fig. 2B), which

227   was resolved by adjustments to cup positions and so appeared independent of the

228   amplifying system.

229   Practical use of the ATONA requires a choice of baseline length, frequency, and, if it is

230   measured with an active sample, magnet position. The short-term stability of the baseline

231   over periods of hours (Fig. 1) suggests that a sufficiently long measurement of the baseline

232   prior to or after sample analysis might be adequate to characterise it accurately. Avoiding

233   repeated block-by-block baseline measurements has the obvious benefit of maximising the

234   on-peak time and thus shortening total analysis time. We tested whether the baseline is

235   entirely electronic, or whether there is any quantifiable contribution from samples on

236   heated filaments, specifically for Pb isotopes (Fig. 3A). We found the baseline to be

237   identical within uncertainty in all configurations: with the LOS (line-of-sight) valve open or

238   closed, with and without a sample, and both on and off peak. The results show that, at least

239   for zone-refined Re filaments and small Pb aliquots, the baseline measurement could be

240   entirely detached from sample analysis. We therefore suggest that ATONA baselines can

241   be measured periodically between sample analyses or e.g. during filament warmup, which

242   will result in time savings without the loss of accuracy. The improvement of baseline

243   accuracy is significant particularly in the first minutes of measurement (Fig. 3B), but

244   accurate analyses of signals close to baseline might require significantly extended baseline

245   acquisition times (Supplementary Fig. 1). For our initial tests presented here, we chose to

246   acquire 600 s of baseline for each of S1, S2 (Table 1). However, if the baseline is isolated

247   from sample analysis, there is no constraint on its acquisition time, and it should ideally be

248   extended from minutes to hours.

249

3.2   Gain stability

251   Precision and accuracy of Faraday measurements is also linked to the stability of inter-

252   channel gain values over the period of an analysis. Similarly to traditional resistor-based

253   amplifiers, the gain of the ATONA is calibrated by comparing the response of individual

254   amplifiers to a fixed reference current applied sequentially to each channel to derive

255   amplifier 'gain factors.' In the ATONA controlling software, gain calibration is fully

256   automated to acquire data over a period of 1–4 h. We performed 4 h gain calibrations over

257   the course of 9 months at a typical rate of 3 every week (Table 2). The results show

258   excellent reproducibility of the 4 h gain means over this period, with single channel values

259   within ~0.6 ppm (1 SD). We observed only a minimal long-term drift with the gain means of

260   month 9 being up to 1 ppm higher than in month 1. The remarkable gain stability of the

261   ATONA implies that there is little need for frequent gain calibrations; we suggest that a re-

262   calibration on a weekly to monthly basis is sufficient to ensure accuracy for routine

263   operation. On a timescale of a single analysis of 2–6 h, the average gain factor will be

264   accurate to within 0.5 ppm; however, with our data we cannot evaluate the possibility of

265   additional scatter added to results as a function of short-term gain variability.

266

3.3   Response time

268   The manufacturer's stated ATONA amplifier decay time is < 0.5 s. Our tests confirm rapid

269   decay from an 8 V U peak top to baseline half-mass away from the peak (< 5 ppm of peak

270   intensity) within 0.5 s for all channels. This fast response time is a key advantage over 10^{13} Ω

271   resistor-based amplifiers[18] in that it allows for significantly shorter (1–2 s) delays following

272   magnet jumps in dynamic methods, as well as efficient focussing.

273

3.4   Pb isotopes

275   Precision and accuracy of ATONA-Faraday Pb isotope measurements were tested with

276   multiple static analyses of 200 pg loads of NIST SRM 982 over a range of intensities (Fig. 4).

277   We acquired data at intensities relevant to single-grain zircon U–Pb geochronology,

278   ranging from run average 200 mV (relative to 10^{11} Ω) to 0.8 mV on ^{208}Pb, corresponding to

279   between ca. 6 mV and 20 μV of ^{204}Pb, respectively. The results at different ATONA

280   integration times are compared with data acquired with the Daly/photomultiplier on the

281   same instrument (Fig. 4). All data in are plotted for 1h total analysis time (rather than total

282   integration time) which illustrates best the practical time efficiency of both detector

283   choices; note, however, that total integration time for each peak in peak-hopping Daly

284   measurements was 3–6 times shorter than in the static Faraday method (5 s for $^{206-208}$Pb, 10

285   s for ^{204}Pb).

286   The precision of both Faraday and Daly measurements (Fig. 4A–B) decreases with average

287   intensity, but it is primarily limited by the intensity of the lower abundance isotope included

288   in the ratio ('limiting beam size'). We found little difference in precision for the three tested

289   integration times of 30, 60, and 100 s; the gain of increasing the integration time to 60 s and

290   beyond might be marginally more pronounced at the lowest intensities closest to baseline.

291   Measuring SRM 982 for isotope ratios of different magnitude allowed us to explore two

292   separate regions of intensity. The high-intensity area (^{208}Pb/^{207}Pb = 2.14, Fig. 4A) illustrates

293   that for 1 h analysis time, Faraday analyses outperform ion counting Daly at all tested

294   integration times for a limiting beam (^{207}Pb) intensity of > 1 mV (ca. 60 kcps). Conversely,

295   the low-intensity region (^{206}Pb/^{204}Pb = 36.7, Fig. 4B) illustrates that Faradays deliver worse

296   precision than the Daly for limiting (^{204}Pb) intensities < 500 μV (ca. 30 kcps). Overall, these

297   results show that the ATONA-Faraday system can provide similar precision to ion counting

298   at average run intensities of 0.5–1 mV (and will clearly outperform it at >1 mV), which

299   significantly expands the applicability of Faraday analyses to pg-sized Pb samples.

300   Fig. 4C additionally illustrates the accuracy of $^{206}Pb/^{204}Pb$ analyses shown in Fig. 4B. The

301   data shows a good degree of consistency in the region described above as advantageous

302   for Faraday analyses (> 500 μV) but with increasing proximity to baseline, low signal/noise

303   leads to scatter outside of internal uncertainty. At limiting intensities < 40 μV (signal/noise

304   < 80), 30–100 s integration time is not sufficient to guarantee accuracy so applications to

305   such small beams should explore significantly extended on-peak and baseline integration

306   times.

307

3.5   Zircon geochronology

309   To evaluate the efficacy of the ATONA in routine U–Pb geochronology applications, we

310   analysed a suite of synthetic U–Pb solutions and fragments of megacrystic zircon GZ7 (Fig.

311   5). The samples varied in size from 1.7 pg Pb* (radiogenic Pb) to 1.4 ng Pb* for the largest

312   fragment of GZ7, and 30 pg–13 ng U. Because for ^{205}Pb-spiked samples the precision and

313   accuracy of most U–Pb dates is dominated by the measurements of ^{206}Pb and ^{207}Pb relative

314   to ^{205}Pb, the main parameter affecting the quality of an analysis is the intensity of the lower

315   of the two signals in each pair ($^{206}Pb/^{205}Pb$, $^{207}Pb/^{205}Pb$). All of our solutions and most GZ7

316   samples had $^{206}Pb/^{205}Pb$ >1 and $^{207}Pb/^{205}Pb$ < 1; only the smallest aliquots of GZ7 had

317    $^{206}Pb/^{205}Pb$ <1. For a typical 10–20 pg ^{205}Pb added from the spike we could routinely

318   maintain an average intensity of 1–3 mV on ^{205}Pb, which placed most $^{206}Pb/^{205}Pb$

319   measurements in a region where static ATONA routines begin to outperform ion counting

320   (Fig. 4). For $^{207}Pb/^{205}Pb$, this was the case only for solution samples. U analyses were never

321   intensity-limited as even for the smallest pg-level samples we could maintain a $^{270}(UO_2)$

322   intensity of 0.5–1 mV.

323

Synthetic solutions

325   Eight large aliquots of ET 4567-R, the most radiogenic of a series of solutions

326   approximating the age of the solar system[24], returned a highly reproducible weighted-

327   mean (n = 8) $^{207}Pb/^{206}Pb$ date of 4559.81 ± 0.27 Ma (MSWD = 0.51; Fig. 5A). The absolute

328   accuracy of dates for this solution is limited primarily by blank subtraction; however, the

329   data shows that for analyses that are not signal-limited (> 1 mV on all major peaks), the

330   ATONA FaraDaly setup is able to produce $^{207}Pb/^{206}Pb$ dates that are reproducible at the 60

331   ppm level for Pb loads of > 50 pg.

332   The EARTHTIME 2 Ga solution[23] was measured for a range of load sizes with a fixed

333   spike/sample ratio giving $^{206}Pb/^{205}Pb = 1.7$, $^{207}Pb/^{205}Pb = 0.2$. While the precision of

334   individual measurements did vary with sample size (11–178 pb Pb*) and intensity (^{205}Pb =

335   1.3–15 mV; see Supplementary Table), all analyses produced results that are

336   indistinguishable at 2s level for all three available U–Pb isotope pairs (Fig. 5B).

337

Zircon GZ7

339   Fragments of zircon GZ7[14] were prepared in two separate batches in order to maintain a

340   standard sample/spike ratio while sequentially decreasing sample size to a minimum of 1.7

341   pg Pb* (Fig. 5C). The precision and accuracy of the results scales with intensity of the

342   limiting beam (itself a function of Pb* and sample ionisation), either ^{205}Pb or ^{206}Pb for

343    $^{206}Pb/^{238}U$ dates (Fig. 5D), or ^{207}Pb for $^{207}Pb/^{235}U$ dates. The average limiting intensities

344   relevant to $^{206}Pb/^{238}U$ dates varied from 5.3 mV to 250 µV (Supplementary Table). Data

345   obtained at limiting intensities > ca. 1 mV overlap previous results obtained for large

346   quantities of the refence material, both internally (Princeton University weighted mean of

347   530.24 ± 0.10 Ma, n = 9) and across five laboratories involved in the Nasdala et al. study[14]

348   (grand mean of 530.26 ± 0.05 Ma, n = 31). Conversely, at intensities < 1 mV the results show

349   scatter outside of the field defined as the reference value, initially without a significant loss

350   of precision (Fig. 5D). This effect might be caused by baseline subtraction as small

351   inaccuracies in baseline quantification might translate into per mil level ratio differences at

352   beam sizes < 1 mV (Supplementary Fig. 1). However, as Daly precision becomes superior to

353   Faraday measurements below ~ 1 mV (Fig. 4B), we suggest that ion counting remain the

354   method of choice for intensities lower than this approximate cut-off value.

355

Oxide correction for UO_2^+

357   The real-time UO_2 oxide correction using mass 269 could be used for a vast majority of ET-

358   spiked U–Pb samples measured over the course of the study. For measurements at the

359   chosen integration time of 30 s, we applied the correction to signals with a sustained

360   intensity of at least 25 mV (2.5×10^{-13} A) on mass 267, which corresponds to ~100 µV (10^{-15}

361   A) on mass 269. This lower limit of intensity was easily achieved for most samples

362   containing ca. 1–3 ng spike ^{235}U; however, it is clear that reliable data for $^{18}O/^{16}O$ can also be

363   obtained at lower intensities, particularly if the integration time is extended beyond 30 s.

364   The accuracy of the oxide correction can be evaluated with a compilation of individual

365   within-run mean $^{18}O/^{16}O$ values measured with our method, on both natural zircons and

366   synthetic U–Pb solutions (Fig. 6). We observed no clear within-run variability of $^{18}O/^{16}O$ (cf.

367   refs 11, 12, 28). The long-term average $^{18}O/^{16}O$ in our analyses was 0.002051 ± 0.000010 (1s,

368   n = 93) which is within uncertainty of atmospheric oxygen values[27] or the range of naturally

369 observed compositions summarised in IUPAC reports.[34] The value is also in agreement with

370 the findings of refs 11,12 who relied on measuring $^{272}(UO_2)$ to correct for the interference.

371 This data shows that the ability to measure small ion beams in any Faraday cup (e.g. with

372 the ATONA or with high-ohmic resistors) significantly expands the repertoire of methods in

373 which such interferences can be accurately corrected, whether using mass 269 or another

374 cup configuration entirely. As in some cases the uncertainty on $^{18}O/^{16}O$ can become a

375 significant source of final uncertainty of U–Pb dates[11], it is clear that analytical

376 improvements in high-precision ID-TIMS geochronology should include this correction

377 routinely as part of UO_2 analysis protocols.

378

Practical application of ATONA to U–Pb geochronology

380 Faraday cups equipped with ATONA amplifiers are ideally suited to analyses of Pb isotopes

381 in a range of radiogenic samples, either of sufficient age or size, with > ca. 10 pg Pb*. For

382 typical amounts of ^{205}Pb spike that produce a sustained 1–3 mV ^{205}Pb, the precision and

383 accuracy is limited by the amount of radiogenic ^{206}Pb and ^{207}Pb available. FaraDaly

384 measurements of old or large U–Pb samples (Fig. 5) are clearly advantageous to ion

385 counting in terms of time, achievable precision and available dynamic range. However, for

386 young zircon U–Pb geochronology that focusses on $^{206}Pb/^{238}U$ dating, samples amenable to

387 our FaraDaly method must meet two criteria: (1) ^{206}Pb beam of at least 1 mV, (2) ^{207}Pb

388 beam that guarantees accuracy even if $^{207}Pb/^{235}U$ dates are only used to assess

389 concordance. As for many young samples the precision and accuracy of $^{207}Pb/^{235}U$ dates is

390 primarily controlled by blank correction rather than measurement precision, we suggest

391 that in such applications ^{207}Pb intensities of > 0.1 mV should be sufficient to evaluate

392 concordance. A possible alternative could be a second magnet jump allowing to analyse

393 ^{207}Pb in the Daly; however, this would add additional time to the analysis. We suggest an

394 integration time of at least 30 s for both Pb and U analyses. Extending the integration time

395 might make smaller beams available due to decreased noise (Fig. 1); however, our SRM 982

396 data (Fig. 4) suggests diminishing returns for integration times beyond ca. 60 s.

397

4   Conclusions

399 We evaluated the performance of the new ATONA system on the Princeton University

400 Isotopx Phoenix TIMS in analyses of Pb and U isotopes in small samples (1.7 pg to 1.4 ng Pb,

401 30 pg to 13 ng U) relevant to routine U–Pb ID-TIMS geochronology. Optimised ATONA

402 FaraDaly routines with $^{202, 205–208}Pb$ in Faraday cups and ^{204}Pb in the Daly-photomultiplier

403 gave precise, reproducible results for all natural and synthetic zircon-like samples

404 producing a sustained limiting intensity of > ca. 1 mV (10^{-14} A), corresponding to ca. 10 pg

405 Pb*. An average intensity of 1 mV on the mass of interest can therefore be considered a

406 practical lower limit of applicability of ATONA to Pb isotopic analyses without a penalty to
407 either precision or accuracy. Additionally, we presented an optimised UO_2 routine taking
408 advantage of the low noise of the ATONA to acquire mass 269 in order to correct in real
409 time for interferences caused by ^{18}O-bearing UO_2 isotopologues.

410 The main benefits of the new ATONA amplifying system for U–Pb geochronology can be
411 summarised as follows: (1) dynamic range exceeding that of any ion counting or resistor-
412 based Faraday amplification system, (2) superior time-normalised precision (vs. Daly) for all
413 ratios with limiting beams of > 1 mV (ca. 60 kcps), (3) outstanding stability of gain, noise,
414 and cup efficiency effectively obviating the need to recalibrate any part of the detector
415 system, and (4) availability for all channels without the need to swap amplifiers (cf. ref. 21).
416 For practical purposes, the advantages of using the ATONA for U–Pb geochronology are
417 similar to those of 10^{13} Ω amplifiers[11,21] but with a greater degree of flexibility in cup
418 configuration, shorter response time, larger dynamic range and better gain stability.

419 The excellent performance of new generations of Faraday cup amplifiers, either the
420 ATONA tested here or traditional design high-ohmic resistors, holds promise of improving
421 both internal and inter-lab reproducibility of highest-precision U–Pb geochronology by ID-
422 TIMS. Together with other analytical improvements, increased use of Faraday collection
423 might be key to the quest of 0.01% reproducibility of ID-TIMS dating as we interrogate
424 geological time in an ever-increasing amount of detail.

425

426

Appendix: UO_2^+ oxide correction for ^{233}U–^{235}U spikes using mass 269

428

429 UO_2^+ measurements of ^{233}U–^{235}U-spiked samples (e.g. using the EARTHTIME ET(2)535
430 tracer) require a correction to account for an interference of $^{233}U^{18}O^{16}O$ and $^{233}U^{16}O^{18}O$ on
431 $^{235}U^{16}O_2$ at mass 267. A correction can be implemented in real time using the data
432 acquisition software, provided the oxygen isotopic composition of UO_2 ($^{18}O/^{16}O = R_{18}$) is
433 assumed or measured. For ^{233}U–^{235}U tracers, a peak of $^{235}U^{18}O^{16}O+^{235}U^{16}O^{18}O+^{233}U^{18}O^{18}O$ at
434 mass 269 is ideally suited to determine R_{18} by relying on an ^{18}O-bearing ion generated with
435 a spike-derived isotope (^{235}U) whose amount is relatively invariable between routinely run
436 samples.

437 Given raw UO_2^+ intensities (i265, i267, i269, and i270), the oxygen isotopic composition R_{18}
438 and oxide corrections involving ^{18}O species ($^{17}O/^{16}O$ being negligibly small) can be obtained
439 simultaneously by solving:

440

441
$$\begin{cases} R_{18} = \dfrac{^{18}O}{^{16}O} = \dfrac{1}{2} \times \dfrac{i269_{oc}}{i267_{oc}} \\ i267_{oc} = i267 - 2 \times R_{18} \times i265 \\ i269_{oc} = i269 - R_{18}^{2} \times i265 \end{cases} \#(1\text{-}3)$$

442

443   where $i267_{oc}$ is $i267$ corrected for interferences of $^{233}U^{18}O^{16}O$ and $^{233}U^{16}O^{18}O$, and $i269_{oc}$ is

444   $i269$ corrected for the minor $^{233}U^{18}O_2$. Solving for R_{18} and $i267_{oc}$ gives:

445

446
$$R_{18} = \frac{i267 - \sqrt{i267^2 - 3 \times i265 \times i269}}{3 \times i265} \#(4)$$

447

448   and

449
$$i267_{oc} = \frac{i267 + 2\sqrt{i267^2 - 3 \times i265 \times i269}}{3} \#(5)$$

450

451   Consequently, output oxide-corrected U isotopic ratios ready for further data reduction

452   (e.g. mass fractionation correction) can be expressed as:

453

454
$$\left(\frac{^{233}U}{^{235}U}\right)_{oc} = \frac{i265}{i267_{oc}} = \frac{3\left(\frac{^{265}UO_2}{^{267}UO_2}\right)}{1 + 2\sqrt{1 - 3\left(\frac{^{265}UO_2}{^{267}UO_2}\right)\left(\frac{^{269}UO_2}{^{267}UO_2}\right)}} \#(6)$$

455

456
$$\left(\frac{^{238}U}{^{235}U}\right)_{oc} = \frac{i270}{i267_{oc}} = \frac{3\left(\frac{^{270}UO_2}{^{267}UO_2}\right)}{1 + 2\sqrt{1 - 3\left(\frac{^{265}UO_2}{^{267}UO_2}\right)\left(\frac{^{269}UO_2}{^{267}UO_2}\right)}} \#(7)$$

457   and

458
$$R_{18} = \frac{1 - \sqrt{1 - 3\left(\frac{^{265}UO_2}{^{267}UO_2}\right)\left(\frac{^{269}UO_2}{^{267}UO_2}\right)}}{3\left(\frac{^{265}UO_2}{^{267}UO_2}\right)} \#(8)$$

459
460
461

462

Figure captions

Figure 1. Measured ATONA current noise across different integration times compared to theoretical Johnson–Nyquist noise of 10^{11}, 10^{12}, and 10^{13} Ω resistor amplifiers (calculated at 20 °C). Noise is defined as 1 SD of baseline.

Figure 2. Variability of 10 s baseline and noise (1 SD of baseline) since installation. Acquisition time 1 h, n = 104.

Figure 3. ATONA baseline settings. A. Comparison of 30 s ATONA baselines measured for 1 h with different combinations of axial mass (204.5 and 205.0, Ax–H4 cups at single mass unit spacing) and opening of the line-of-sight (LOS) valve, with and without a heated, ^{205}Pb-spiked zircon sample. B. Compilation of baseline data illustrating the improvement of baseline accuracy with acquisition time. Colour-coding of channels is identical to Fig. 1. 1 aA = 10^{-18} A. Error bars in A are 1 SD.

Figure 4. Precision and accuracy of NIST SRM 982 analyses across a range of intensities. Faraday runs were acquired in static mode for 1 h (not including 2 × 300 s baseline); Daly runs employed peak-hopping between ^{204}Pb, ^{206}Pb, ^{207}Pb, ^{208}Pb for a total of 1h analysis time. All intensities are reported relative to a 10^{11} Ω resistor. The limiting beam in A is ^{207}Pb, in B it is ^{204}Pb.

Figure 5. ATONA U–Pb geochronology results for synthetic solutions and natural zircon reference material GZ7. All uncertainties are displayed at 2s level. The grey band around concordia represents uncertainty bounds of U decay constants.[33] Within the GZ7 dataset, blue-green symbols are zircon fragments spiked and dissolved individually, purple represents small (1.7–5.8 pg Pb*) sub-samples of a single shard aliquoted and spiked post-

499 dissolution; limiting intensity (D) is the lower of ^{206}Pb, ^{205}Pb. Synthetic solution data

500 displays similar trends as in D, but does not access the < 1 mV region (all intensity data

501 available in the Supplementary Table).

502

503 Figure 6. Results of R_{18} determinations from UO_2 analyses of natural zircons and synthetic

504 U–Pb solutions following methods described in section 2.3 and equations in the Appendix.

505 The average value over the course of the study was 0.002051± 0.000010 (1s), which is

506 comparable to the composition of atmospheric oxygen[27] and in good agreement with

507 results from other labs.[11,12]

508

509

510

511 **References**

512

513 1.   M. D. Schmitz, in *The Geologic Time Scale*, eds. F. M. Gradstein, J. G. Ogg, M. D. Schmitz
514   and G. M. Ogg, Elsevier, Boston, 2012, pp. 115–126.
515 2.   B. Schoene, in *Treatise on Geochemistry*, eds. H. D. Holland and K. K. Turekian, Elsevier,
516   Oxford, 2nd edn., 2014, pp. 341–378.
517 3.   U. Schaltegger, A. Schmitt and M. Horstwood, *Chem. Geol.*, 2015, **402**, 89–110.
518 4.   A. O. Nier, *Rev. Sci. Instrum.*, 1940, **11**, 212–216.
519 5.   A. O. Nier, *Rev. Sci. Instrum.*, 1947, **18**, 398–411.
520 6.   A. O. Nier, R. W. Thompson and B. F. Murphey, *Phys. Rev.*, 1941, **60**, 112.
521 7.   C. Patterson, *Geochim. Cosmochim. Acta*, 1956, **10**, 230–237.
522 8.   G. R. Tilton, C. Patterson, H. Brown, M. Inghram, R. Hayden, D. Hess and E. Larsen Jr, *Geol.*
523   *Soc. Am. Bull.*, 1955, **66**, 1131–1148.
524 9.   T. E. Krogh, *Geochim. Cosmochim. Acta*, 1973, **37**, 485–494.
525 10.   J. M. Mattinson, *Anal. Chem.*, 1972, **44**, 1715–1716.
526 11.   J. F. Wotzlaw, Y. Buret, S. J. E. Large, D. Szymanowski and A. von Quadt, *J. Anal. At.*
527   *Spectrom.*, 2017, **32**, 579–586.
528 12.   D. J. Condon, B. Schoene, N. M. McLean, S. A. Bowring and R. R. Parrish, *Geochim.*
529   *Cosmochim. Acta*, 2015, **164**, 464–480.
530 13.   N. M. McLean, D. J. Condon, B. Schoene and S. A. Bowring, *Geochim. Cosmochim. Acta*,
531   2015, **164**, 481–501.
532 14.   L. Nasdala, F. Corfu, B. Schoene, S. R. Tapster, C. J. Wall, M. D. Schmitz, M. Ovtcharova, U.
533   Schaltegger, A. K. Kennedy, A. Kronz, P. W. Reiners, Y.-H. Yang, F.-Y. Wu, S. E. M. Gain, W.
534   L. Griffin, D. Szymanowski, C. Chanmuang N., M. Ende, J. W. Valley, M. J. Spicuzza, B.
535   Wanthanachaisaeng and G. Giester, *Geostand. Geoanal. Res.*, 2018, **42**, 431–457.
536 15.   J. M. Mattinson, *Chem. Geol.*, 2005, **220**, 47–66.
537 16.   P. Widmann, J. Davies and U. Schaltegger, *Chem. Geol.*, 2019, **511**, 1–10.
538 17.   M. H. Huyskens, S. Zink and Y. Amelin, *Chem. Geol.*, 2016, **438**, 25–35.
539 18.   J. M. Koornneef, C. Bouman, J. B. Schwieters and G. R. Davies, *Anal. Chim. Acta*, 2014, **819**,
540   49–55.
541 19.   M. Klaver, R. J. Smeets, J. M. Koornneef, G. R. Davies and P. Z. Vroon, *J. Anal. At.*
542   *Spectrom.*, 2016, **31**, 171–178.
543 20.   G. Wang, T. Sun and J. Xu, *Rapid Commun. Mass Spectrom.*, 2017, **31**, 1616–1622.

544   21.   A. von Quadt, J. F. Wotzlaw, Y. Buret, S. J. E. Large, I. Peytcheva and A. Trinquier, *J. Anal.*
545   *At. Spectrom.*, 2016, **31**, 658–665.
546   22.   S. E. Cox, S. R. Hemming and D. Tootell, *Geochronology*, 2020.
547   23.   D. J. Condon, N. McLean, B. Schoene, S. Bowring, R. Parrish and S. Noble, *Geochim.*
548   *Cosmochim. Acta*, 2008, **72**, A175.
549   24.   J. N. Connelly and D. J. Condon, presented in part at Goldschmidt Conference, Sacramento,
550   June, 2014.
551   25.   H. Gerstenberger and G. Haase, *Chem. Geol.*, 1997, **136**, 309–312.
552   26.   Y. Amelin and W. Davis, *J. Anal. At. Spectrom.*, 2006, **21**, 1053-1061.
553   27.   A. O. Nier, *Phys. Rev.*, 1950, **77**, 789–793.
554   28.   G. J. Wasserburg, S. B. Jacobsen, D. J. DePaolo, M. T. McCulloch and T. Wen, *Geochim.*
555   *Cosmochim. Acta*, 1981, **45**, 2311–2323.
556   29.   J. Harvey and E. F. Baxter, *Chem. Geol.*, 2009, **258**, 251–257.
557   30.   J. F. Bowring, N. M. McLean and S. A. Bowring, *Geochem. Geophys. Geosyst.*, 2011, **12**,
558   Q0AA19.
559   31.   N. M. McLean, J. F. Bowring and S. A. Bowring, *Geochem. Geophys. Geosyst.*, 2011, **12**,
560   Q0AA18.
561   32.   J. Hiess, D. J. Condon, N. McLean and S. R. Noble, *Science*, 2012, **335**, 1610–1614.
562   33.   A. H. Jaffey, K. F. Flynn, L. E. Glendenin, W. C. Bentley and A. M. Essling, *Phys. Rev. C*, 1971,
563   **4**, 1889–1906.
564   34.   J. Meija, T. B. Coplen, M. Berglund, W. A. Brand, P. De Bièvre, M. Gröning, N. E. Holden, J.
565   Irrgeher, R. D. Loss, T. Walczyk and T. Prohaska, *Pure Appl. Chem.*, 2016, **88**, 293–306.
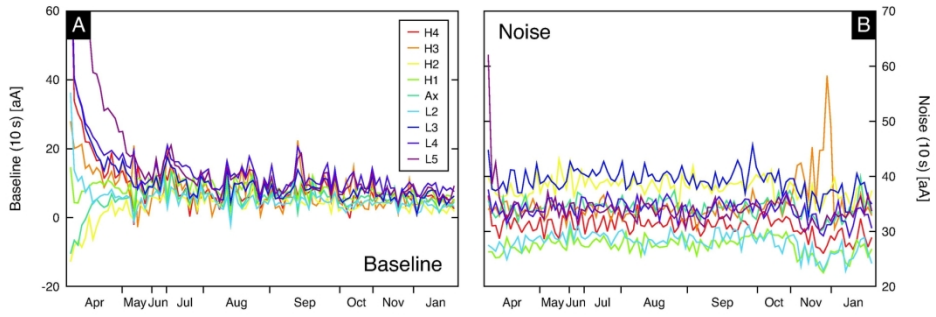
1
2
3
4
5
6
7
8
9
10
11
12
13
14
15
16
17
18
19
20
21
22
23
24
25
26
27
28
29
30
31
32
33
34
35
36
37
38
39
40
41
42
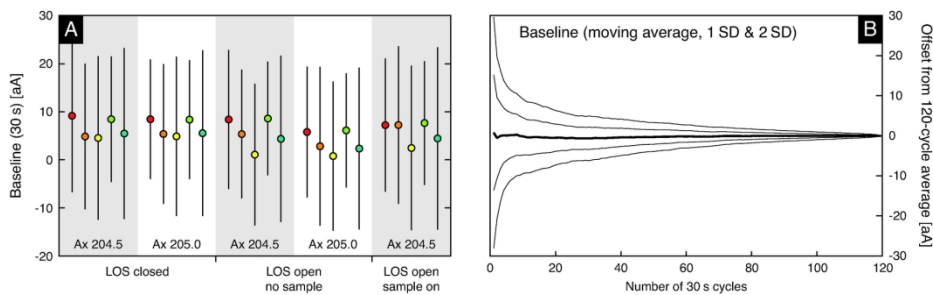43
44
45
46
47
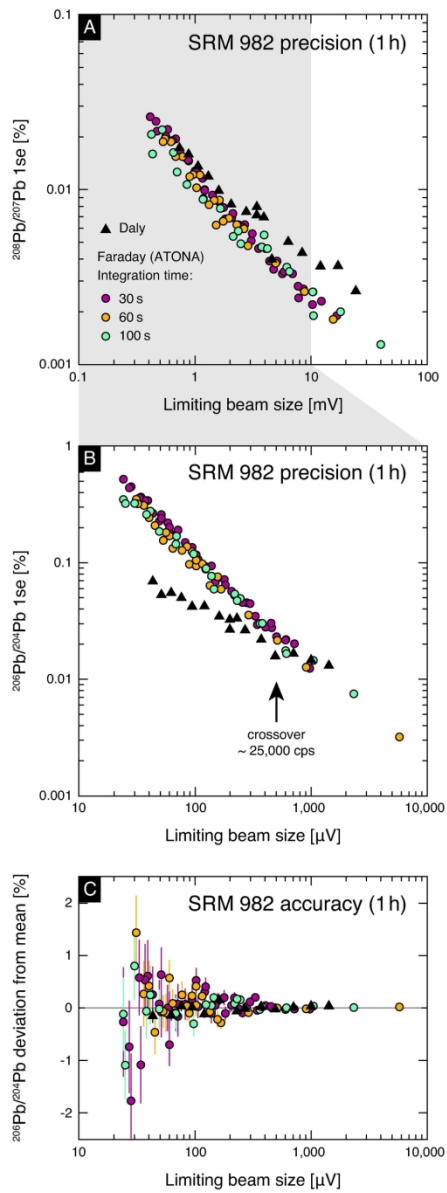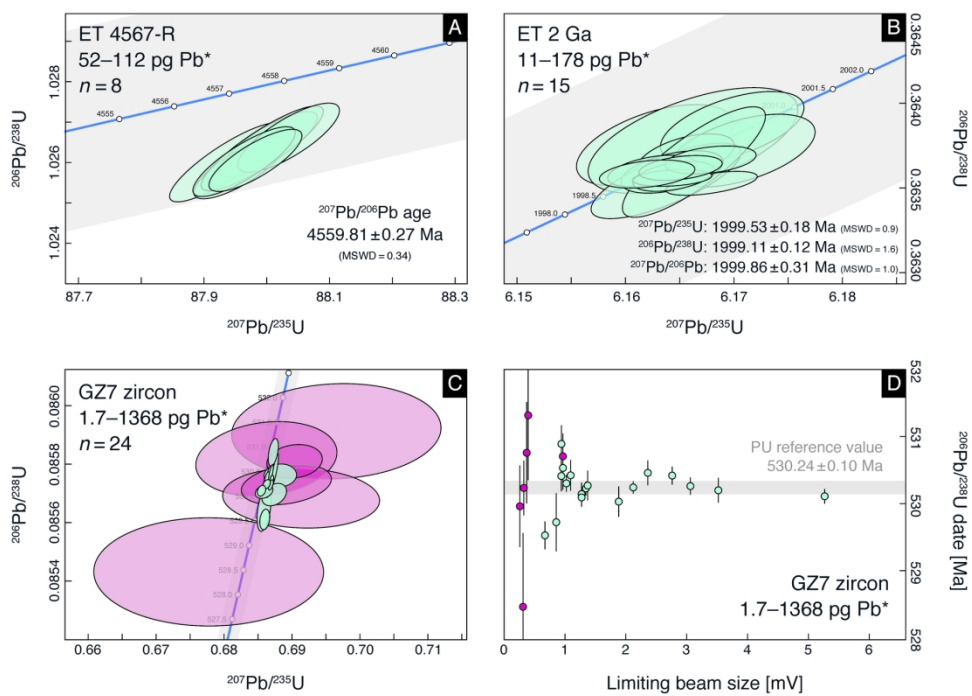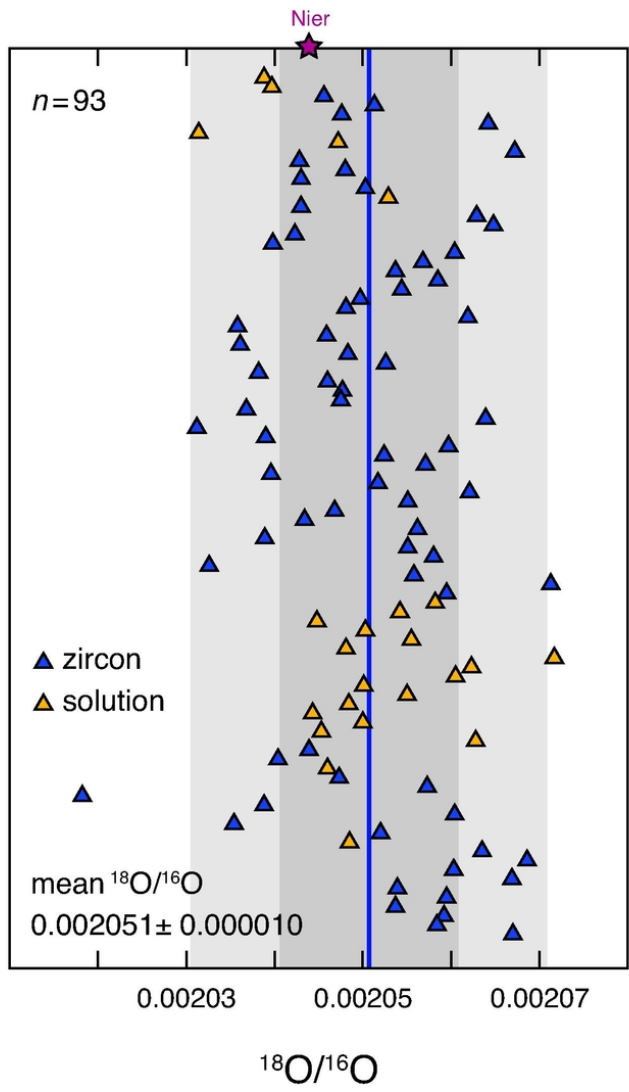48
49
50
51
52
53
54
55
56
57
58
59
60

Table 1. Collector configurations used for Pb and UO_2 analyses

Method		L5	L4	L3	L2	Ax	PM	H1	H2	H3	H4
Pb NBS 982						^{204}Pb			^{206}Pb	^{207}Pb	^{208}Pb
Pb zircon	S1				^{202}Pb		^{204}Pb	^{205}Pb	^{206}Pb	^{207}Pb	^{208}Pb
	S2							^{205}Pb	^{206}Pb	^{207}Pb	^{208}Pb
UO_2 zircon		$^{265}(UO_2)$	$^{267}(UO_2)$	$^{269}(UO_2)$	$^{270}(UO_2)$						

Table 2. Results of ATONA amplifier gain calibration runs (acquisition time 4 h) over the course of 9 months (n = 152)

Channel	Gain	1 RSD, ppm
H4	0.99441867	0.58
H3	1.00660676	0.60
H2	1.01282664	0.57
H1	1.00965005	0.56
Ax	1.00280493	0.61
L2	1.00645470	0.62
L3	1.00654362	0.61
L4	1.00121184	0.55
L5	1	
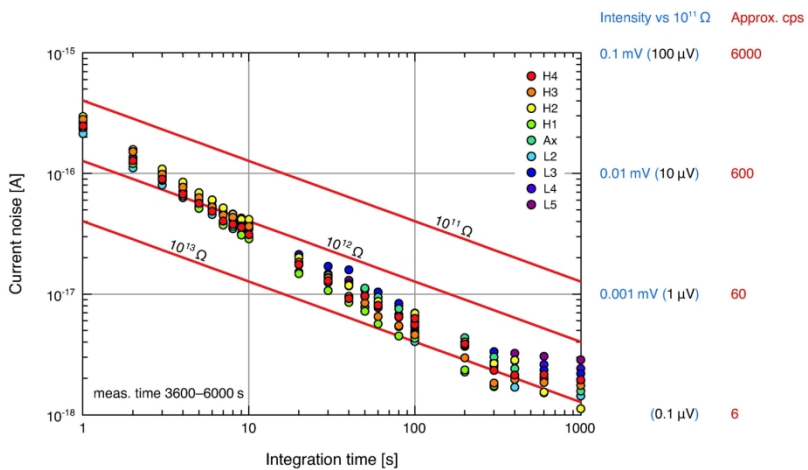
Fig1

170x88mm (300 x 300 DPI)

Fig2

170x74mm (300 x 300 DPI)

Fig3

170x53mm (300 x 300 DPI)

Fig4

82x224mm (300 x 300 DPI)

Fig5

171x125mm (300 x 300 DPI)

Fig6

82x96mm (300 x 300 DPI)